UR-3490-1573

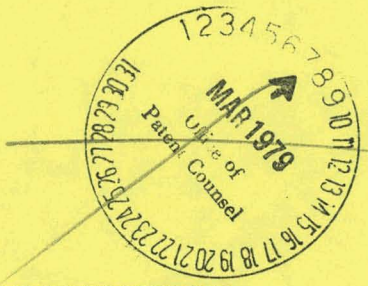

VISUALIZATION OF DRUG-NUCLEIC ACID INTERACTIONS AT ATOMIC RESOLUTION

IV. STRUCTURE OF AN AMINOACRIDINE/ DINUCLEOSIDE MONOPHOSPHATE CRYSTALLINE COMPLEX, 9-AMINOACRIDINE: 5-IODOCYTIDYLYL(3'-5')GUANOSINE

by

T. D. Sakore, B. S. Reddy and Henry M. Sobell

Department of Chemistry
River Campus Station
The University of Rochester
Rochester, New York 14627

Department of Radiation Biology
and Biophysics
The University of Rochester School
of Medicine and Dentistry
Rochester, New York 14642

DISCLAIMER

ABSTRACT:

9-Aminoacridine forms a crystalline complex with the dinucleoside monophosphate, 5-iodocytidylyl(3'-5')guanosine (iodoCpG). These crystals are monoclinic, space group $P2_1$, with $\underline{a}$ = 13.98 Å, $\underline{b}$ = 30.58 Å, $\underline{c}$ = 22.47 Å and β = 113.9°. The structure has been solved to atomic resolution by Patterson and Fourier methods, and refined by a combination of Fourier and sum function Fourier methods. The asymmetric unit contains four 9-aminoacridine molecules, four iodoCpG molecules and 21 water molecules, a total of 245 atoms. 9-Aminoacridine demonstrates two different intercalative binding modes and, along with these, two slightly different intercalative geometries in this model system.

The first of these is very nearly symmetric, the 9-amino- group lying in the narrow groove of the intercalated base-paired nucleotide structure. The second shows grossly asymmetric binding to the dinucleotide, the 9-amino- group lying in the wide groove of the structure. Associated with these two different intercalative binding modes is a difference in geometries in the structures. Although both structures demonstrate C3' endo (3'-5') C2' endo mixed sugar puckering patterns (i.e., both cytidine residues have C3' endo sugar conformations, while both guanosine residues have C2' endo sugar conformations), with corresponding twist angles between base-pairs of about 10°, they differ in the magnitude of the helical screw axis dislocation accompanying intercalation (Sobell et al., 1977a, b). In the pseudosymmetric intercalative structure, this value is about +0.5 Å, whereas in the asymmetric intercalative structure this value is about +2.7 Å. These conformational differences can be best described as a "sliding" of base-pairs on the intercalated acridine molecule.

Although the pseudosymmetric intercalative structure can be used in 9-aminoacridine-DNA binding, the asymmetric intercalative structure cannot since this poses

ABSTRACT: (continued)

stereochemical difficulties in connecting neighboring sugar-phosphate chains to the intercalated dinucleotide. It is possible, however, that the asymmetric binding mode is related to the mechanism of 9-aminoacridine induced frameshift mutagenesis (Sakore et al., 1977), and we discuss this possibility here in further detail.

RUNNING TITLE:

DRUG-NUCLEIC ACID INTERACTIONS IV.

1. Introduction.

9-Aminoacridine (Fig. 1) is one in a class of aminoacridines that has long been known to be a potent frameshift mutagen in viruses and bacteria. The molecule is known to bind to DNA by intercalation (Lerman, 1961, 1963). Its mutagenic activity, however, has been postulated to reflect the stabilization of transiently looped-out single-stranded regions of DNA during DNA replication or repair. Subsequent events (such as musmatch repair or DNA replication) can then give rise to addition- or deletion- type frameshift mutations (Streisinger et al., 1966).

The Streisinger model accounts for the general tendency for frameshift mutations to arise in areas of local base-sequence redundancy, and for frameshift mutational hot spots to occur in DNA regions that have short repetitive base sequences (Streisinger et al., 1966; Okada et al., 1972). It also accounts for the general tendency for frameshift mutations to arise in the vicinity of strand discontinuities (as occurs, for example, at the ends of chromosomes or near replication forks) (Linstrom & Drake, 1970; Newton et al., 1972). According to this model, however, the mutagenicity of intercalating agents (such as 9-aminoacridine) reflects an indirect effect of stabilizing looped out base configurations through stacking interactions with individual bases, rather than by intercalation into double-helical DNA per se.

This paper describes the structure of a crystalline complex containing 9-aminoacridine and the self-complementary dinucleoside monophosphate, 5-iodocytidylyl(3'-5')guanosine (Fig. 2). The structure demonstrates <u>two</u> intercalative binding modes in this model system. The first of these involves a pseudosymmetric stacking interaction between 9-aminoacridine molecules and guanine-cytosine base-pairs. The second configuration is an asymmetric interaction, governed largely

by stacking forces between acridine and guanine rings. We postulate this second type of association to play an important role in the origin of frameshift mutagenesis and advance a possible mechanism. A preliminary account of this work has appeared elsewhere (Sakore et al., 1977).

2. Materials and Methods.

9-Aminoacridine was purchased from K & K Laboratories, Inc., Plainview, New York and used without further purification. The dinucleoside monophosphate, cytidylyl(3'-5')guanosine, was obtained as the ammonium salt from Sigma Chemical Co. and then iodinated using a synthesis described previously (Tsai et al., 1977). Plate-like yellow crystals were obtained by slow evaporation over several days of equimolar mixtures of 9-aminoacridine and 5-iodocytidylyl(3'-5')guanosine dissolved in a 50% water/methanol (vol/vol) solvent system. Spectral studies indicated a complex containing equimolar quantities of both compounds. Space group and unit cell dimensions were initially obtained from precession photographs with nickel-filtered CuKα radiation, and then refined by least squares from 12 independent reflections measured on a Picker FACS-1 automatic diffractometer. The crystals are monoclinic, space group $P2_1$, with $\underline{a}$ = 13.98 ± 0.02 Å, $\underline{b}$ = 30.58 ± 0.04 Å, $\underline{c}$ = 22.47 ± 0.03 Å, β = 113.9 ± 0.4°.

Data were collected at room temperature with Ni-filtered CuKα radiation out to a two-theta angle of 72° , using the theta-two theta scan method. For this purpose, a single crystal of the complex (0.2 mm x 0.3 mm x 0.5 mm) was mounted along the $\underline{a}$ axis in a 1.0 mm glass capillary with some mother liquor. Of 4418 measured reflections, 2251 were significantly above background (i.e., 1.5σ). The intensities were corrected for the Lorentz and polarization factors. No absorption corrections were used. The overall isotropic temperature factor and scale factor were derived by Wilson (1942) statistics. Normalized structure

factors were then calculated using the K-curve method (Karle & Hauptman, 1953) and used to calculate an (E^2-1) map. The initial interpretation of this map gave only two iodine positions unambiguously. These were then used to calculate a Patterson superposition map using a minimum function -- this gave two additional iodine positions that were consistent with the (E^2-1) Patterson map. All four iodine positions were then reconfirmed by calculating additional Patterson superposition maps using two iodines at a time. This method also revealed the positions of two cytosine rings, three phosphorous atoms and fragments of several ribose sugars. Phases calculated from this partial structure were then used in a sum-function Fourier synthesis (where amplitudes are $(|2F_o|-|F_c|)$ and the phases are the calculated phases to generate additional information. The complete structure was eventually developed after computing a large number of Fourier, difference Fourier and sum-function Fourier syntheses, often leaving out portions of the structure that were either unclear or in doubt and allowing them to reappear in later Fourier maps. This minimized bias in the structure analysis and assisted the Fourier refinement. The final structure contains 245 atoms in the asymmetric unit: four aminoacridines, four iodoCpG molecules, and 21 water molecules. Individual isotropic temperature factors for carbon, nitrogen and oxygen atoms and anisotropic temperature factors for iodine atoms were then refined using several cycles of block diagonal least squares. The final residual is 14.7% for 2251 reflections.

The observed and calculated structure factors have been microfilmed and stored at ASIS/NAPS c/o Microfiche Publications, P.O. Box 3513, Grand Central Station, New York, New York 10017 under document number 00000.

3. Results.

Tables 1 and 2 summarize final coordinates and temperature factors obtained from this crystal structure analysis. Estimated standard deviations for x, y and z coordinates of light atoms lie between 0.04 and 0.05 Å. This results in rather large standard deviations for bond lengths and angles in this structure analysis (estimated standard deviations for bond lengths is ± 0.1 Å; for bond angles, ± 5°), probably reflecting the size of the structure and the limited data available.

(a) 9-aminoacridine demonstrates two different drug-nucleic acid intercalative binding modes.

Figures 3-10 show portions of the asymmetric unit of the 9-aminoacridine-5-iodocytidylyl(3'-5')guanosine crystal structure as determined by this study. The structure contains two 2:2 aminoacridine-iodoCpG complexes, each forming miniature Watson-Crick intercalated structures that stack along the a axis to form infinite sandwich-like columns of acridine molecules and guanine-cytosine base-pairs.

In the first part of the asymmetric unit, the intercalated 9-aminoacridine molecule is oriented such that its amino- group points towards the narrow groove of the miniature double helix. The stacked 9-aminoacridine molecule, however, is oppositely oriented and lies above and below guanine-cytosine base-pairs of the intercalated dinucleoside monophosphate. A different situation exists in the second part of the asymmetric unit. Here, the intercalated 9-aminoacridine molecule is oriented such that its amino- group lies in the wide groove of the double helix. The stacked 9-aminoacridine molecule is similarly oriented, its amino-group again pointing towards the wide groove.

An important additional difference between these 2:2 complexes is the

stacking mode that is observed between the acridine molecules and guanine-cytosine base-pairs. In the first complex, the intercalated aminoacridine molecule is pseudo-symmetric with respect to the base-pairs, while in the second complex a distinctly asymmetric stacking pattern exists. Accompanying this second asymmetric intercalative binding mode is a large shift in ring overlap between guanine-cytosine base-pairs, as viewed in projection (compare Fig. 3, 4 and 7, 8). This conformational difference is best described as a 'sliding' of base-pairs upon the intercalated acridine molecule.

(b) Sugar-phosphate conformations accompanying drug intercalation.

Table 3 summarizes the values of torsional angles that describe the sugar-phosphate conformations in the structure. In both the symmetric and asymmetric intercalative complexes, the iodocytidine ribose sugar residues are best described by C3' endo and the guanosine sugar residues as C2' endo (Sundaralingam, 1965). In each case, the conformation around the C4'-C5' bond is gauche-gauche. The glycosidic torsional angles (denoted χ) fall in the low anti range for iodocytidine residues, while these fall in the high anti range for guanosine residues. This correlation between the glycosidic torsional angles and the sugar puckering has been observed in a large number of crystal structures of individual nucleosides and nucleotides (Sundaralingam, 1969), and has also be observed in a detailed study of transfer RNA (Jack et al., 1976). A similar correlation exists in the refined structures of A and B DNA (Arnott and Hukins, 1972).

Our data does not allow us to specify the specific changes in torsional angles in the sugar-phosphate backbone that allow the 'sliding' of base-pairs upon the intercalated acridine molecule, a feature observed in the asymmetric acridine-iodoCpG complex. Model building studies, however, suggest this con-

formational difference to primarily reflect changes in the glycosidic torsional angles of both guanosine and iodocytidine residues (χ values for both nucleosides decrease; guanosine, from about 110 to 80 , iodocytidine, from about 35 to 10). We hesitate to be too confident on this point, however.

We have also calculated the twist angle relating base-pairs above and below the intercalative 9-aminoacridine molecule in both pseudosymmetric and asymmetric complexes (this value has been calculated by projecting the inter-glycosidic carbon vectors on a common plane and then measuring the angle between them). These values are both very similar: $10 \pm 2^{\circ}$ for the pseudosymmetric structure, $8 \pm 2^{\circ}$ for the asymmetric structure. The small magnitude of this angular twist reflects the presence of the intercalative aminoacridine molecule and the detailed nature of the sugar-phosphate geometry. The value is close to that observed in other drug-dinucleoside monophosphate crystalline complexes (Tsai et al., 1977; Jain et al., 1977; Wang et al., 1978; Reddy et al., 1979; Jain et al., 1979)

Stereo- pairs of the pseudosymmetric and asymmetric intercalative geometries are shown in Fig. 11 and 12.

(c) Lattice structure.

Fig. 13 shows the 9-aminoacridine-iodoCpG structure viewed down the a axis. The structure consists of separate columns of 9-aminoacridine-iodoCpG pseudosymmetric and asymmetric intercalative complexes related by a pseudo- 2-fold screw at y = 1/4 and 3/4 stabilized through hydrogen bonding with numerous water molecules. A total of 21 water molecules have been located in the asymmetric unit, many of these forming water-water tetrahedral-like structures. Other water molecules form water-hydroxyl linkages to the sugar-phosphate chains and hydrophillic groups of base-pairs and 9-aminoacridine molecules.

The relevant hydrogen bonding contacts observed in this structure have been summarized in Table 4.

4. Discussion.

The mechanism of aminoacridine induced frameshift mutagenesis is a subject that has attracted a great deal of interest over the years (see Drake & Baltz, 1976, for a review). Frameshift mutations consist of additions and deletions of varying numbers of base-pairs (not integral multiples of three, however). Although usually of the +1 or -1 type, larger additions and deletions occur with reasonable frequency (Terzaghi et al., 1966; Okada et al., 1969; Imada et al., 1970; Ocada et al., 1970).

The most plausible model to explain frameshift mutagenesis is a model proposed by Streisinger and his colleagues several years ago to explain the amino acid changes in a variety of plus-minus intragenically suppressed mutants of phage T4 lysozyme (Streisinger et al., 1966). In this model (shown schematically in Fig. 14A), looped-out single stranded DNA regions arise transiently during DNA replication and repair through local melting and reannealing of DNA chains in regions having short repetitive base sequences or local base-sequence redundancies -- such transient structures can then be stabilized through further DNA synthesis. Addition- or deletion- type frameshift mutations arise through subsequent DNA replication or mismatch repair.

How then do the aminoacridines induce frameshift mutagenesis?

Streisinger et al., 1966 have suggested these agents to bind to looped-out single stranded DNA regions that arise spontaneously during DNA replication or repair -- this would tend to stabilize these regions and promote the series of events described above. According to this model, therefore, the mutagenicity of these intercalating agents reflects the secondary effect of stabilizing preexisting

single-stranded DNA regions through stacking interactions with individual bases rather than by intercalation into double-helical DNA per se.

Our studies of drug intercalation, however, have suggested an alternative (although similar) mechanism to understand aminoacridine induced frameshift mutagenesis. This model postulates DNA to exist in a second prereplicative form during DNA replication or repair -- this structure (denoted β kinked DNA) is one of a series of DNA unwinding structural intermediates that exist at the replication fork during DNA synthesis ahead of the DNA polymerase enzyme (Sobell et al., 1978; Sobell, 1978). As DNA unwinds, kinks open to assume intercalative geometry and this results in the appearance of tight binding sites for intercalative drugs and dyes. In the case of the aminoacridine dyes, these molecules begin by first binding to these sites asymmetrically (the reader should study the acridine orange- and proflavine- DNA binding models presented in the accompanying paper (Reddy et al., 1979)). These then slide over to bind to single-stranded premelted DNA regions as unwinding continues (see Fig. 14B). The presence of dye molecules transiently bound to single-stranded DNA immediately in front of the DNA polymerase enzyme causes slippage of the enzyme upon the template -- this results in the formation of looped-out single stranded DNA regions that can be stabilized through further DNA synthesis. Again, addition- or deletion- type frameshift mutations arise through subsequent DNA replication or mismatch repair.

It is important to note that our model predicts the formation of these looped-out regions to be caused by frameshift mutagens -- and, for this reason, directly relates the phenomenon of drug intercalation to frameshift mutagenesis. Our model makes the fundamental physical prediction that frameshift mutagens bind double helical DNA asymmetrically, remaining attached to single-stranded DNA as DNA unwinds. Covalently attached intercalating chemical carcinogens could have

similar pharmacological action (Levine et al., 1974; Cole, 1970).

This study has provided evidence for two different intercalative binding modes in the 9-aminoacridine-iodoCpG model drug-nucleic acid interaction (see Fig. 15A and B). The pseudosymmetric intercalative configuration can be readily utilized by 9-aminoacridine when it intercalates into double-helical DNA. The asymmetric intercalative structure, on the other hand, cannot be utilized for drug intercalation into the double helical DNA polymer -- this reflects the magnitude of the helical screw axis dislocation that would have to accompany this binding mode (i.e., 2.7 Å for the asymmetric binding mode, compared to 0.5 Å for the pseudosymmetric binding mode) (Sobell et al., 1977a, b), and the resulting difficulties in connecting neighboring sugar-phosphate chains with the intercalated dinucleotide structure.

How then do we envision 9-aminoacridine to cause frameshift mutagenesis?

According to our model, 9-aminoacridine begins by intercalating into DNA at the replication fork either pseudosymmetrically or asymmetrically -- the latter resembling acridine orange- or proflavine- DNA binding (Reddy et al., 1979). As DNA continues to unwind, the asymmetric intercalative binding mode tends to persist, becoming even more asymmetric as DNA chains begin to separate -- it is possible that the geometry observed for the asymmetric 9-aminoacridine-iodoCpG complex is relevant here. Finally, 9-aminoacridine molecules slide over to single-stranded premelted DNA regions -- held transiently through stacking interactions with bases and electrostatic interactions with phosphate oxygens. Other steps in our mechanism remain the same as described earlier.

We are continuing to study other aminoacridine-dinucleoside monophosphate interactions in an effort to obtain further information concerning symmetric or asymmetric binding. We will report on these at a later time.

Acknowledgements:

This work has been supported by grants from the National Institutes of Health, the American Cancer Society and the Department of Energy. This paper has been assigned report no. UR-0000-0000 at the DOE, the University of Rochester.

REFERENCES:

Arnott, S. & Hukins, D. W. L. (1969). Nature (London), 224, 886-888.

Cole, R. S. (1970). Biochim. Biophys. Acta, 217, 30-

Drake, J. W. & Baltz, R. H. (1976). Ann. Rev. Biochem. 45, 11-37.

Imada, M., Inouye, M., Eda, M. & Tsugita, A. (1970). J. Mol. Biol. 54, 199-217.

Jack, A., Ladner, J. E. & Klug, A. (1976). J. Mol. Biol. 108, 619-649.

Jain, S. C., Tsai, C. -C. & Sobell, H. M. (1977). J. Mol. Biol. 114, 317-331.

Karle, J. & Hauptman, H. (1953). Acta Cryst. 6, 473-476.

Lerman, L. S. (1961). J. Mol. Biol. 3, 18-30.

Lerman, L. S. (1963). Proc. Nat. Acad. Sci. USA, 49, 94-102.

Levine, A. F., Fink, L. M., Weinstein, I. B. & Grunberger, D. (1974). Cancer Res. 34, 319-327.

Linstrom, D. M. & Drake, J. W. (1970). Proc. Nat. Acad. Sci. USA, 65, 617-624.

Newton, A., Masys, D., Leonardi, E. & Wygal, D. (1972). Nature New Biol. 236, 19-23.

Ocada, Y., Amagase, S. & Tsugita, A. (1970). J. Mol. Biol. 54, 219-246.

Okada, Y., Streisinger, G., Emrich, J., Tsugita, A. & Inouye, M. (1969). J. Mol. Biol. 40, 299-304.

Okada, Y., Streisinger, G., Owen, J., Newton, J., Tsugita, A. & Inouye, M. (1972) Nature (London), 236, 338-341.

Reddy, B. S., Seshadri, T. P., Sakore, T. D. & Sobell, H. M. (1979). J. Mol. Biol. (in press).

Sakore, T. D., Jain, S. C., Tsai, C. -C. & Sobell, H. M. (1977). Proc. Nat. Acad. Sci. USA, 74, 188-192.

Sobell, H. M., Tsai, C. -C., Jain, S. C. & Gilbert, S. G. (1977a). J. Mol. Biol. 114, 333-365.

Sobell, H. M., Reddy, B. S., Bhandary, K. K., Jain, S. C., Sakore, T. D. & Seshadri, T. P. (1977b). Cold Spring Harb. Symp. Quant. Biol. 42, 87-102.

Sobell, H. M., Lozansky, E. D. & Lessen, M. (1978). Cold Spring Harb. Symp. Quant. Biol. 43, 000-000.

Sobell, H. M. (1978). in Biological Regulation and Development, Volume 1, ed. R. F. Goldberger, Plenum Publishing Corporation, New York, New York pp. 000-000.

REFERENCES: (continued)

Streisinger, G., Okada, Y., Emrich, J., Newton, J., Tsugita, A., Terzaghi, E. & Inouye, M. (1966). Cold Spring Harb. Symp. Quant. Biol. 31, 77-84.

Sundaralingam, M. (1965). J. Amer. Chem. Soc. 87, 599-606.

Sundaralingam, M. (1969). Biopolymers, 7, 821-860.

Tsai, C. -C., Jain, S. C. & Sobell, H. M. (1977). J. Mol. Biol. 114, 301-315.

Wilson, A. J. C. (1942). Nature (London), 150, 151-152.

FIGURE CAPTIONS:

Figure 1. Chemical structure of 9-aminoacridine.

Figure 2. Chemical structure of 5-iodocytidylyl(3'-5')guanosine.

Figure 3. A computer drawn illustration of the first part of the asymmetric unit of the 9-aminoacridine-iodoCpG crystal structure viewed approximately parallel to the planes of the guanine-cytosine base-pairs and 9-aminoacridine molecules. IodoCpG molecules are drawn with dark solid bonds; intercalative and stacked 9-aminoacridine molecules are drawn with light open bonds. A pseudosymmetric intercalating binding mode is observed in this portion of the asymmetric unit. Bond distances of sugar-phosphate chains are shown in this figure.

Figure 4. Same as Fig. 3, but showing bond angles of sugar-phosphate chains.

Figure 5. Illustration of the first part of the asymmetric unit of the 9-aminoacridine-iodoCpG crystal structure viewed perpendicular to the planes of the guanine-cytosine base-pairs and 9-aminoacridine molecules, showing bond distances of base-pairs and 9-aminoacridine molecules. For simplicity, the bond distances of only one base-pair are shown; the other base-pair has very similar bond distances and angles.

Figure 6. Same as Fig. 5 but showing bond angles of base-pairs and 9-aminoacridine molecules.

Figure 7. A computer drawn illustration of the second part of the asymmetric unit of the 9-aminoacridine-iodoCpG crystal structure viewed approximately parallel to the planes of the guanine-cytosine base-pairs and 9-aminoacridine molecules. IodoCpG molecules are drawn with dark solid bonds; intercalative and stacked 9-aminoacridine molecules are drawn with light open bonds. An asymmetric intercalation binding mode is observed in this portion of the asymmetric unit. Bond distances of sugar-phosphate chains are shown in this figure.

Figure 8. Same as Fig. 7, but showing bond angles of sugar-phosphate chains.

Figure 9. Illustration of the second part of the asymmetric unit of the 9-aminoacridine-iodoCpG crystal structure viewed perpendicular to the planes of the guanine-cytosine base-pairs and 9-aminoacridine molecules, showing bond distances of base-pairs and 9-aminoacridine molecules. For simplicity, the bond distances of only one base-pair are shown; the other base-pair has very similar bond distances and angles.

Figure 10. Same as Fig. 9, but showing bond angles of base-pairs and 9-aminoacridine molecules.

Figure 11. Stereo- pairs of the pseudosymmetric 9-aminoacridine-iodoCpG intercalative binding mode.

FIGURE CAPTIONS: (continued)

Figure 12. Stereo- pairs of the asymmetric 9-aminoacridine-iodoCpG intercalative binding mode.

Figure 13. A lattice picture of the 9-aminoacridine-iodoCpG crystalline complex viewed down the a crystallographic direction to show relationships between columns of 9-aminoacridine: iodoCpG complexes and the surrounding water structure.

Figure 14. (a) Streisinger model to explain the origin of aminoacridine induced frameshift mutagenesis. Mutagens, such as the aminoacridines, are postulated to stabilize transiently looped-out single stranded DNA regions that arise spontaneously during replication or repair. Subsequent events (such as mismatch repair or DNA replication) can then give rise to addition- or deletion- type frameshift mutations.

(b) Alternate model to explain the origin of aminoacridine induced frameshift mutagenesis. DNA is postulated to exist in a second pre-replicative form during DNA replication or repair -- this structure (denoted β kinked DNA) is one of a series of DNA unwinding structural intermediates that exist at the replication fork during DNA synthesis ahead of the DNA polymerase enzyme. As DNA unwinds, kinks open to assume intercalative geometry and this results in the appearance of tight binding sites for intercalative drugs and dyes. In the case of the aminoacridine dyes, these molecules begin by first binding to these sites asymmetrically -- these then slide over to bind to single-stranded premelted DNA regions as unwinding continues. The presence of these dye molecules transiently bound to single-stranded DNA immediately in front of the DNA polymerase enzyme causes slippage of the enzyme upon the template -- this results in the formation of looped-out single stranded DNA regions that can be stabilized through further DNA synthesis. Again, addition- or deletion- type frameshift mutations arise through subsequent DNA replication or mismatch repair.

See text for additional discussion.

Figure 15. Illustration summarizing the two different intercalative binding modes observed in the 9-aminoacridine-iodoCpG crystalline complex.

(a) Pseudosymmetric intercalative binding mode.

(b) Asymmetric intercalative binding mode.

Table 1. Final coordinates and temperature factors for 9-aminoacridine-iodoCpG crystal structure. 5-iodocytidylyl(3'-5')guanosine molecules.

NO.	ATOM	X/A	Y/B	Z/C	B	NO.	ATOM	X/A	Y/B	Z/C	B
				5-IODOCYTIDYLYL(3'-5')GUANOSINE							
		IODO-CPG(1)						IODO-CPG(2)			
1	I5C1	-0.2868	0.6968	-0.2241	7.8	42	I5C2	0.3008	0.7500	0.2743	7.9
2	N1C1	-0.3984	0.8275	-0.2578	3.5	43	N1C2	0.2888	0.8858	0.2222	11.0
3	C2C1	-0.3834	0.8417	-0.1967	3.3	44	C2C2	0.2666	0.8850	0.1555	6.1
4	N3C1	-0.3400	0.8167	-0.1455	7.9	45	N3C2	0.2565	0.8442	0.1233	2.3
5	C4C1	-0.3167	0.7750	-0.1533	5.7	46	C4C2	0.2665	0.8041	0.1577	3.3
6	C5C1	-0.3325	0.7583	-0.2133	1.3	47	C5C2	0.2889	0.8050	0.2244	8.1
7	C6C1	-0.3767	0.7834	-0.2645	5.2	48	C6C2	0.2972	0.8467	0.2556	6.4
8	O2C1	-0.4066	0.8808	-0.1889	1.7	49	O2C2	0.2610	0.9192	0.1266	8.1
9	N4C1	-0.2806	0.7500	-0.0978	7.3	50	N4C2	0.2499	0.7667	0.1233	1.4
10	C1'C1	-0.4501	0.8542	-0.3133	6.8	51	C1'C2	0.3165	0.9266	0.2578	16.9
11	C2'C1	-0.3750	0.8833	-0.3278	1.8	52	C2'C2	0.2333	0.9466	0.2778	10.5
12	C3'C1	-0.3554	0.8626	-0.3834	13.9	53	C3'C2	0.2610	0.9291	0.3445	12.1
13	C4'C1	-0.4501	0.8342	-0.4167	2.6	54	C4'C2	0.3777	0.9291	0.3723	7.8
14	O1'C1	-0.5000	0.8250	-0.3700	4.6	55	O1'C2	0.4084	0.9167	0.3178	10.6
15	C5'C1	-0.4417	0.7958	-0.4555	4.9	56	C5'C2	0.4304	0.8984	0.4278	10.1
16	O5'C1	-0.3611	0.7667	-0.4111	5.2	57	O5'C2	0.4166	0.8517	0.4056	8.4
17	O2'C1	-0.4501	0.9208	-0.3611	4.3	58	O2'C2	0.2500	0.9950	0.2744	8.0
18	O3'C1	-0.3443	0.8875	-0.4389	7.4	59	O3'C2	0.2332	0.9583	0.3834	5.1
19	P1	-0.2267	0.8796	-0.4388	7.0	60	P2	0.1325	0.9417	0.3914	8.0
20	O1P1	-0.2278	0.9083	-0.4922	15.8	61	O1P2	0.1001	0.9666	0.4389	8.1
21	O1P2	-0.2304	0.8326	-0.4555	16.3	62	O2P2	0.1333	0.8934	0.3956	11.1
22	O5'G1	-0.1417	0.8875	-0.3668	9.0	63	O5'G2	0.0417	0.9437	0.3167	8.0
23	C1'G1	0.1304	0.8917	-0.2423	1.1	64	C1'G2	-0.2369	0.9392	0.1900	2.0
24	C2'G1	0.1351	0.8881	-0.3073	14.9	65	C2'G2	-0.2558	0.9388	0.2506	18.7
25	C3'G1	0.0823	0.9297	-0.3384	4.0	66	C3'G2	-0.1771	0.9773	0.2817	7.0
26	C4'G1	0.0000	0.9375	-0.3090	3.3	67	C4'G2	-0.1068	0.9884	0.2434	14.4
27	O1'G1	0.0250	0.9083	-0.2533	4.8	68	O1'G2	-0.1403	0.9583	0.1932	13.1
28	C5'G1	-0.1176	0.9328	-0.3487	14.1	69	C5'G2	0.0072	0.9827	0.2745	18.8
29	O2'G1	0.2405	0.8880	-0.3025	20.2	70	O2'G2	-0.3643	0.9517	0.2432	20.8
30	O3'G1	0.1434	0.9637	-0.3496	9.6	71	O3'G2	-0.2531	1.0116	0.2806	20.7
31	N1G1	0.2033	0.8508	-0.0111	6.4	72	N1G2	-0.3055	0.8500	-0.0178	2.0
32	C2G1	0.1883	0.8933	-0.0389	7.4	73	C2G2	-0.3138	0.8950	-0.0111	6.3
33	N3G1	0.1733	0.8950	-0.1034	5.2	74	N3G2	-0.2958	0.9133	0.0466	4.2
34	C4G1	0.1666	0.8550	-0.1345	5.7	75	C4G2	-0.2666	0.8842	0.0967	1.1
35	C5G1	0.1749	0.8150	-0.1078	6.1	76	C5G2	-0.2542	0.8408	0.0922	1.3
36	C6G1	0.1999	0.8125	-0.0445	4.1	77	C6G2	-0.2733	0.8216	0.0334	5.2
37	O6G1	0.2083	0.7750	-0.0178	4.2	78	O6G2	-0.2633	0.7825	0.0289	3.6
38	N2G1	0.1945	0.9316	-0.0088	6.3	79	N2G2	-0.3499	0.9217	-0.0633	2.7
39	N7G1	0.1639	0.7833	-0.1556	1.2	80	N7G2	-0.2300	0.8192	0.1466	5.2
40	C8G1	0.1499	0.8083	-0.2089	8.2	81	C8G2	-0.2250	0.8542	0.1845	2.1
41	N9G1	0.1471	0.8542	-0.1978	0.7	82	N9G2	-0.2466	0.8942	0.1578	1.8
				5-IODOCYTIDYLYL(3'-5')GUANOSINE							
		IODO-CPG(3)						IODO-CPG(4)			
83	I5C3	0.3447	0.7797	0.7189	9.4	124	I5C4	0.7862	0.7377	0.2350	9.9
84	N1C3	0.4056	0.6442	0.7422	6.8	125	N1C4	0.7917	0.5975	0.2844	4.8
85	C2C3	0.4044	0.6283	0.6834	8.4	126	C2C4	0.8139	0.5950	0.3511	3.9
86	N3C3	0.3917	0.6592	0.6355	5.5	127	N3C4	0.8223	0.6359	0.3822	3.1
87	C4C3	0.3710	0.7025	0.6455	10.1	128	C4C4	0.8167	0.6767	0.3478	3.8
88	C5C3	0.3711	0.7175	0.7044	26.3	129	C5C4	0.7973	0.6791	0.2834	1.6
89	C6C3	0.3863	0.6866	0.7523	12.3	130	C6C4	0.7862	0.6383	0.2533	13.3
90	O2C3	0.4251	0.5892	0.6745	4.1	131	O2C4	0.8222	0.5600	0.3778	5.7
91	N4C3	0.3570	0.7317	0.6000	7.8	132	N4C4	0.8278	0.7150	0.3834	5.3
92	C1'C3	0.4306	0.6116	0.7944	12.4	133	C1'C4	0.7834	0.5550	0.2505	1.1
93	C2'C3	0.5418	0.5950	0.8267	15.2	134	C2'C4	0.6751	0.5400	0.2334	7.5
94	C3'C3	0.5834	0.6250	0.8822	5.3	135	C3'C4	0.6278	0.5600	0.1678	5.2
95	C4'C3	0.4960	0.6316	0.9056	5.4	136	C4'C4	0.7084	0.5483	0.1411	10.4
96	O1'C3	0.4000	0.6291	0.8444	11.2	137	O1'C4	0.8056	0.5625	0.1944	6.0
97	C5'C3	0.5042	0.6792	0.9278	7.3	138	C5'C4	0.6973	0.5850	0.0922	8.0
98	O5'C3	0.4500	0.7083	0.8945	20.8	139	O5'C4	0.6833	0.6333	0.1022	7.5
99	O2'C3	0.5501	0.5458	0.8334	5.3	140	O2'C4	0.6890	0.4917	0.2333	5.6
100	O3'C3	0.6751	0.6042	0.9333	4.6	141	O3'C4	0.5499	0.5275	0.1333	8.7
101	P3	0.7988	0.6167	0.9462	5.1	142	P4	0.4333	0.5450	0.1210	4.3
102	P3O1	0.8000	0.6658	0.9556	16.3	143	P4O1	0.4166	0.5917	0.0944	8.5
103	P3O2	0.8750	0.5958	1.0144	17.5	144	P4O2	0.3667	0.5084	0.0778	5.8
104	O5'G3	0.8167	0.6157	0.8807	9.8	145	O5'G4	0.4167	0.5442	0.1888	4.5
105	C1'G3	0.9203	0.5958	0.7405	8.8	146	C1'G4	0.2916	0.5458	0.3000	10.6
106	C2'G3	0.9922	0.6052	0.8090	14.2	147	C2'G4	0.2249	0.5517	0.2277	6.3
107	C3'G3	0.9796	0.5682	0.8453	11.4	148	C3'G4	0.2333	0.5100	0.1943	5.4
108	C4'G3	0.8644	0.5629	0.8134	19.7	149	C4'G4	0.3333	0.4917	0.2443	8.7
109	O1'G3	0.8335	0.5834	0.7490	27.2	150	O1'G4	0.3750	0.5167	0.3055	14.0
110	C5'G3	0.8036	0.5715	0.8524	14.2	151	C5'G4	0.4166	0.5000	0.2166	10.5
111	O2'G3	1.0949	0.6134	0.8131	16.5	152	O2'G4	0.1166	0.5667	0.2110	8.2
112	O3'G3	1.0410	0.5291	0.8612	25.8	153	O3'G4	0.1583	0.4834	0.2111	6.2
113	N1G3	0.8805	0.6333	0.5200	4.5	154	N1G4	0.3583	0.6291	0.5066	4.3
114	C2G3	0.8861	0.5917	0.5456	5.3	155	C2G4	0.3472	0.5833	0.5000	6.2
115	N3G3	0.8972	0.5883	0.6100	6.7	156	N3G4	0.3333	0.5659	0.4600	6.5
116	C4G3	0.9028	0.6275	0.6422	15.0	157	C4G4	0.3330	0.5958	0.3934	10.3
117	C5G3	0.9000	0.6692	0.6167	1.1	158	C5G4	0.3444	0.6400	0.4000	4.5
118	C6G3	0.8888	0.6717	0.5545	9.3	159	C6G4	0.3583	0.6575	0.4589	7.6
119	O6G3	0.8833	0.7083	0.5278	8.1	160	O6G4	0.3750	0.6975	0.4667	5.7
120	N2G3	0.8750	0.5542	0.5133	3.8	161	N2G4	0.3499	0.5559	0.5444	7.4
121	N7G3	0.9085	0.7000	0.6600	12.7	162	N7G4	0.3416	0.6600	0.3444	6.0
122	C8G3	0.9114	0.6767	0.7111	9.3	163	C8G4	0.3276	0.6250	0.3055	12.3
123	N9G3	0.9086	0.6334	0.7022	15.6	164	N9G4	0.3220	0.5850	0.3311	9.7

Table 1. (continued)

Temperature factors shown for iodine atoms are the equivalent isotropic temperature factors calculated from the anisotropic temperature parameters obtained from full matrix least-squares. These are:

	U_{11}	U_{22}	U_{33}	U_{12}	U_{13}	U_{23}
I5C1	0.1276	0.0573	0.0883	0.0135	0.0400	-0.0052
I5C2	0.1256	0.0589	0.0871	0.0000	0.0254	0.0000
I5C3	0.1516	0.0652	0.1213	-0.0034	0.0677	-0.0242
I5C4	0.1522	0.0591	0.1234	-0.0116	0.0266	0.0175

Table 2. Final coordinates and temperature factors for 9-aminoacridine-iodoCpG crystal structure. 9-Aminoacridine molecules.

NO.	ATOM	X/A	Y/B	Z/C	B	NO.	ATOM	X/A	Y/B	Z/C	B
		9-AMINOACRIDINE(1)						9-AMINOACRIDINE(2)			
165	C1 A1	-0.0362	0.9200	0.0612	13.5	180	C1 A2	0.4431	0.8184	-0.0666	11.9
166	C2 A1	-0.0085	0.9091	0.1255	9.9	181	C2 A2	0.4166	0.8515	-0.1144	7.6
167	C3 A1	0.0082	0.8658	0.1433	6.1	182	C3 A2	0.4069	0.8933	-0.1044	7.6
168	C4 A1	-0.0029	0.8333	0.0989	1.5	183	C4 A2	0.4209	0.9083	-0.0445	4.9
169	C5 A1	-0.0831	0.7875	-0.1166	11.2	184	C5 A2	0.5110	0.8775	0.1739	7.5
170	C6 A1	-0.1109	0.7983	-0.1800	9.1	185	C6 A2	0.5347	0.8479	0.2229	10.4
171	C7 A1	-0.1304	0.8417	-0.1989	11.2	186	C7 A2	0.5458	0.8025	0.2134	8.9
172	C8 A1	-0.1165	0.8750	-0.1533	8.6	187	C8 A2	0.5305	0.7875	0.1528	12.1
173	C9 A1	-0.0767	0.8967	-0.0456	7.3	188	C9 A2	0.4874	0.8016	0.0416	8.3
174	N10A1	-0.0001	0.0000	-0.0078	21.0	189	N10A2	0.4667	0.8917	0.0644	9.0
175	C11A1	-0.0722	0.8208	-0.0711	5.9	190	C11A2	0.4943	0.8617	0.1133	7.6
176	C12A1	-0.0861	0.8642	-0.0894	7.0	191	C12A2	0.5027	0.8171	0.1044	6.5
177	C13A1	-0.0472	0.8875	0.0178	5.7	192	C13A2	0.4625	0.8333	-0.0067	9.6
178	C14A1	-0.0333	0.8441	0.0356	9.3	193	C14A2	0.4514	0.8775	0.0044	6.8
179	N9 A1	-0.0917	0.9400	-0.0667	11.3	194	N9 A2	0.4999	0.7600	0.0289	8.1
		9-AMINOACRIDINE(3)						9-AMINOACRIDINE(4)			
195	C1 A3	0.5833	0.6917	0.3489	1.4	210	C1 A4	0.0585	0.6934	0.3767	7.5
196	C2 A3	0.5638	0.6767	0.2867	3.2	211	C2 A4	0.0501	0.6717	0.3200	6.0
197	C3 A3	0.5500	0.6317	0.2744	2.3	212	C3 A4	0.0611	0.6254	0.3167	8.6
198	C4 A3	0.5528	0.6008	0.3222	3.0	213	C4 A4	0.0792	0.6000	0.3722	5.1
199	C5 A3	0.6057	0.5666	0.5434	6.0	214	C5 A4	0.1417	0.5950	0.5934	2.0
200	C6 A3	0.6251	0.5825	0.6044	4.1	215	C6 A4	0.1526	0.6170	0.6500	5.4
201	C7 A3	0.6390	0.6283	0.6167	5.8	216	C7 A4	0.1416	0.6634	0.6511	10.6
202	C8 A3	0.6390	0.6583	0.5689	4.3	217	C8 A4	0.1194	0.6884	0.5978	10.8
203	C9 A3	0.6112	0.6750	0.4589	6.6	218	C9 A4	0.0891	0.6900	0.4867	6.1
204	N10A3	0.5807	0.5833	0.4322	7.6	219	N10A4	0.1085	0.5983	0.4833	11.1
205	C11A3	0.5779	0.6150	0.3845	2.9	220	C11A4	0.0890	0.6225	0.4289	4.8
206	C12A3	0.5917	0.6608	0.3978	7.2	221	C12A4	0.0779	0.6671	0.4311	8.2
207	C13A3	0.6168	0.6442	0.5067	5.4	222	C13A4	0.1084	0.6667	0.5411	6.1
208	C14A3	0.6002	0.5975	0.4945	11.2	223	C14A4	0.1210	0.6200	0.5378	4.6
209	N9 A3	0.6251	0.7184	0.4712	12.9	224	N9 A4	0.0807	0.7383	0.4900	12.8
				SOLVENT MOLECULE ATOMS							
225	OW1	0.0678	0.9881	0.8494	5.9	236	OW12	0.4478	0.9804	0.0639	16.5
226	OW2	0.4774	0.5065	0.7139	12.8	237	OW13	0.5081	0.6801	0.1157	8.9
227	OW3	0.1048	0.8097	0.5516	13.1	238	OW14	0.6077	0.9803	0.5614	10.5
228	OW4	0.1293	0.5155	0.0018	11.8	239	OW15	0.5947	0.8024	0.4034	12.4
229	OW5	0.1555	0.6882	0.9695	19.0	240	OW16	0.6478	0.9667	0.4450	11.0
230	OW6	0.8484	0.7821	0.6632	17.0	241	OW17	0.7709	0.6914	0.0684	7.4
231	OW7	0.2307	0.9370	0.5674	9.9	242	OW18	0.8394	0.8234	0.3598	12.6
232	OW8	0.2392	0.6652	0.1210	16.5	243	OW19	0.9158	0.9602	0.4646	20.6
233	OW9	0.3036	0.7809	0.4534	17.4	244	OW20	0.9867	0.7154	0.0031	13.6
234	OW10	0.3707	0.5055	0.9561	10.8	245	OW21	0.2539	0.6954	0.8374	13.6
235	OW11	0.4167	1.0000	0.6211	8.8						

Table 3. Torsional angles describing conformations of sugar-phosphate chains in 9-aminoacridine-iodoCpG crystalline complex.

Torsional Angle*	Greek symbol	I-CpG(1)	I-CpG(2)	I-CpG(3)	I-CpG(4)
O1'C-C1'C-N1C-C6C	χ	17	38	17	20
O1'G-C1'G-N9G-C8G	χ	109	100	83	102
O5'C-C5'C-C4'C-C3'C	ψ	61	71	99	42
C5'C-C4'C-C3'C-O3'C	ψ'	72	85	99	105
C4'C-C3'C-O3'C-P	ϕ'	236	216	216	209
C3'C-O3'C-P-O5'G	ω'	311	296	310	287
O3'G-P-O5'G-C5'G	ω	280	300	295	294
P-O5'G-C5'G-C4'G	ϕ	220	229	208	222
O5'G-C5'G-C4'G-C3'G	ψ	67	38	58	45
C5'G-C4'G-C3'G-O3'G	ψ'	110	130	106	156
C4'C-O1'C-C1'C-C2'C	τ_0	4	2	10	-4
O1'C-C1'C-C2'C-C3'C	τ_1	-17	-25	-31	-26
C1'C-C2'C-C3'C-C4'C	τ_2	23	37	39	44
C2'C-C3'C-C4'C-O1'C	τ_3	-21	-37	-33	-50
C3'C-C4'C-O1'C-C1'C	τ_4	11	21	13	32
C4'G-O1'G-C1'G-C2'G	τ_0	-34	-26	-30	-24
O1'G-C1'G-C2'G-C3'G	τ_1	42	22	46	30
C1'G-C2'G-C3'G-C4'G	τ_2	-33	-12	-42	-21
C2'G-C3'G-C4'G-O1'G	τ_3	13	-1	23	7
C3'G-C4'G-O1'G-C1'G	τ_4	11	14	5	11

* The torsional angle is defined in terms of 4 consecutive atoms, ABCD; the positive sense of rotation is clockwise from A to D while looking down the BC bond.

Table 4. Hydrogen bonding distances in 9-aminoacridine-iodoCpG crystal structure.

Atoms	Distance (A)
OW1 - O3'G4 (8)	2.89
OW2 - O2C3 (1)	2.68
OW2 - O2'C3 (1)	2.73
OW2 - O2'G2 (11)	2.73
OW3 - N9G4 (1)	2.53
OW4 - N9G1 (10)	2.89
OW4 - O3'G3 (4)	2.92
OW5 - O6G1 (2)	2.74
OW5 - OW20 (5)	2.87
OW6 - N7G3 (1)	2.66
OW6 - O5'C1 (6)	2.76
OW6 - O1P2 (6)	2.89
OW7 - O3'G1 (2)	2.73
OW7 - O1P2 (1)	2.87
OW7 - OW11 (1)	3.06
OW8 - N4C2 (1)	3.10
OW9 - O6G4 (1)	2.71
OW10 - O2P2 (2)	2.71
OW10 - OW12 (11)	2.85
OW10 - N3G2 (9)	3.00
OW11 - N1OG3(12)	2.82
OW11- O2'C1 (6)	2.98
OW12 - N1OG2(1)	2.72
OW12 - O2'C3(12)	3.05
OW13 - O1P4 (1)	2.95
OW13 - O5'C4(1)	2.96
OW13 - N9G2 (1)	3.10
OW14 - N3G4 (12)	2.75
OW14 - O2'G1(6)	2.85
OW14 - OW16 (1)	2.92
OW14 - O3'C1(6)	2.92

Atoms	Distance (A)
OW15 - O5'C2 (1)	2.93
OW15 - N9G3 (1)	2.93
OW16 - O1P1 (6)	2.50
OW16 - N2G4 (12)	2.74
OW17 - O5'C4 (1)	2.50
OW17 - O1P3 (3)	2.84
OW17 - O6G2 (7)	2.90
OW19 - O1P2 (7)	2.86
OW19 - O1P1 (6)	3.01
OW20 - O1P3 (3)	2.82
OW21 - O5'C3 (1)	2.54
OW21 - N7G1 (2)	3.00

(1)	x	y	z
(2)	x	y	z+1
(3)	x	y	z-1
(4)	x-1	y	z-1
(5)	x-1	y	z+1
(6)	x+1	y	z+1
(7)	x+1	y	z
(8)	$\bar{x}$	y+½	$\bar{z}$+1
(9)	$\bar{x}$	y-½	$\bar{z}$+1
(10)	$\bar{x}$	y-½	$\bar{z}$+1
(11)	$\bar{x}$+1	y-½	$\bar{z}$+1
(12)	$\bar{x}$+1	y+½	$\bar{z}$+1

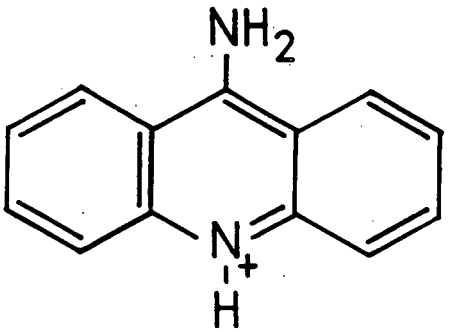

Figure 1.

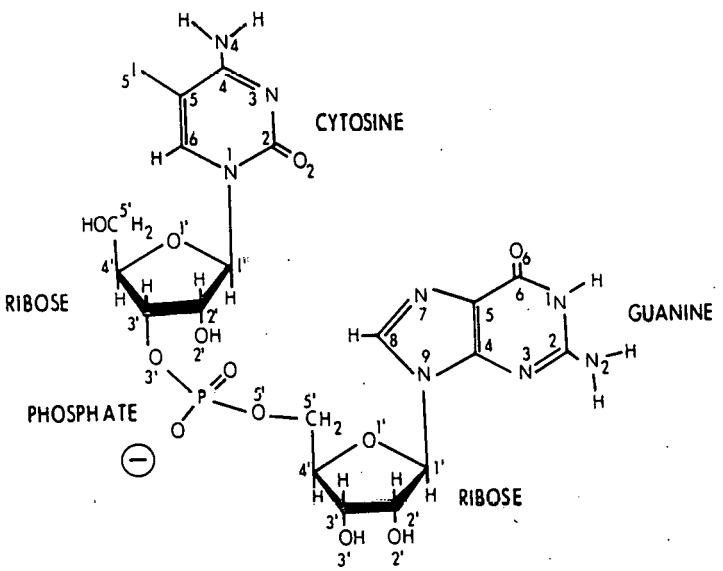

Figure 2.

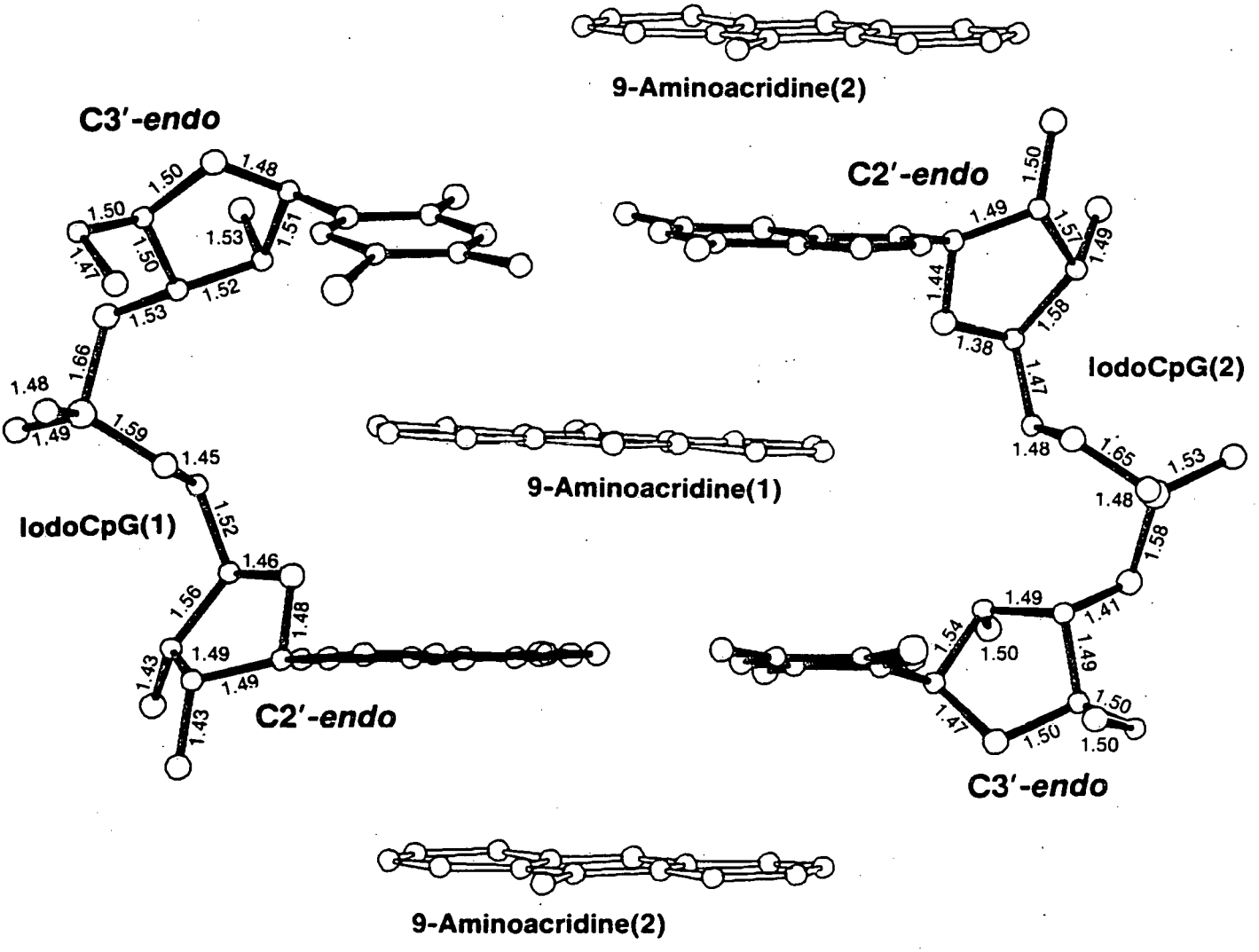
9-Aminoacridine(2)
C3′-endo
C2′-endo
IodoCpG(2)
9-Aminoacridine(1)
IodoCpG(1)
C2′-endo
C3′-endo
9-Aminoacridine(2)

Figure 3.

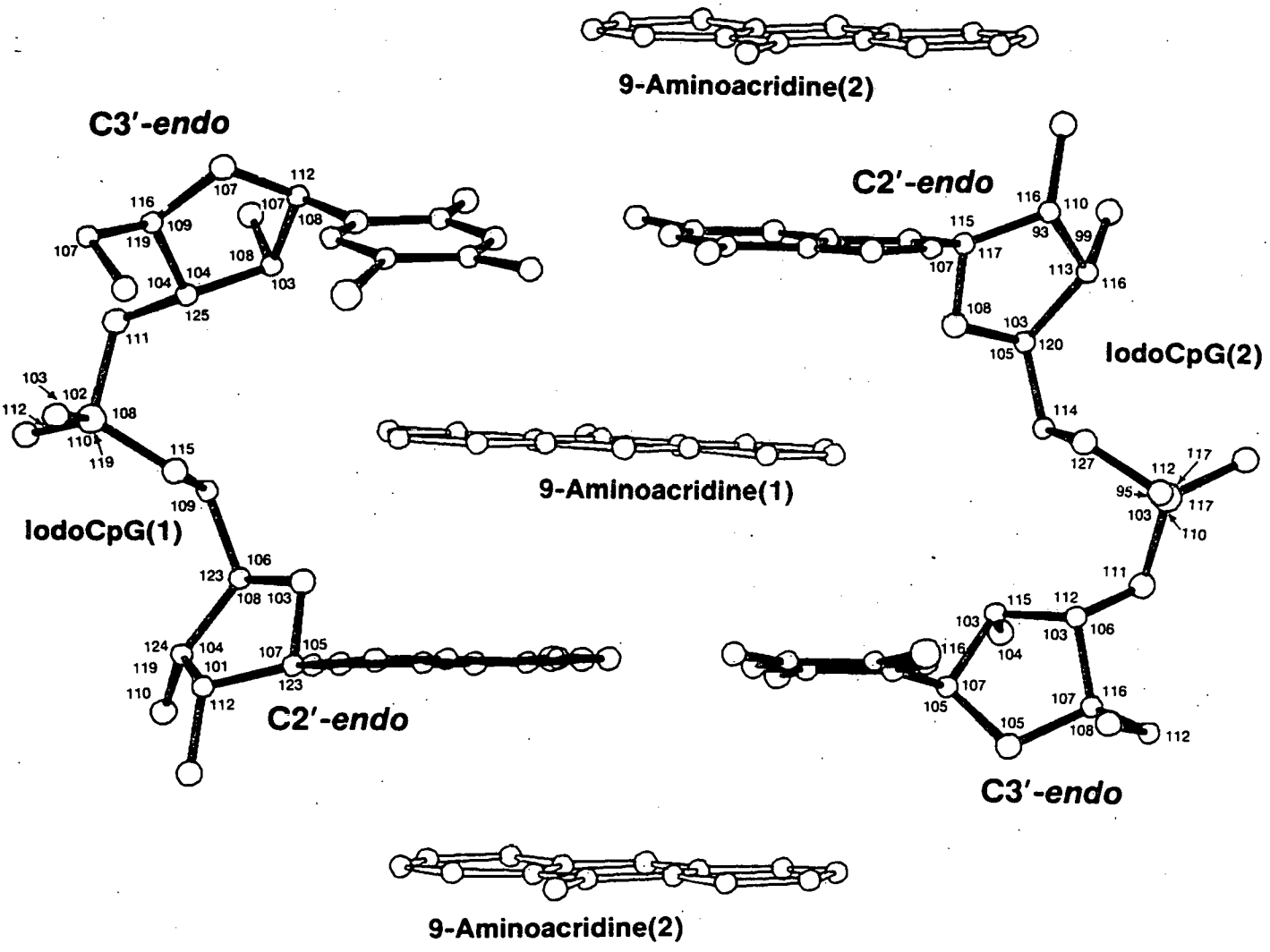
9-Aminoacridine(2)
C3′-endo
C2′-endo
IodoCpG(2)
9-Aminoacridine(1)
IodoCpG(1)
C2′-endo
C3′-endo
9-Aminoacridine(2)

Figure 4.

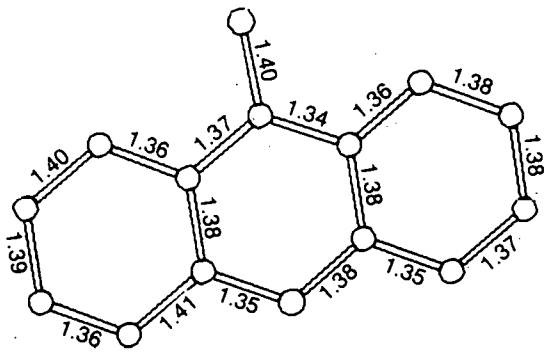

9-Aminoacridine(1)

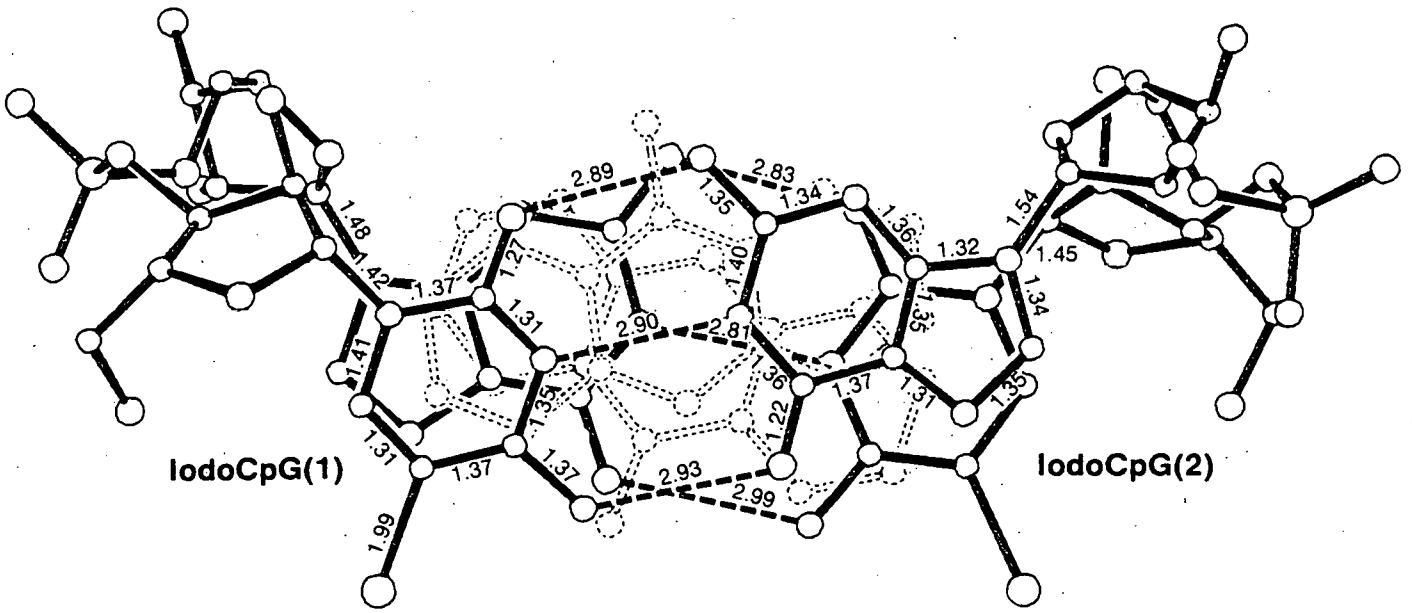

IodoCpG(1)

IodoCpG(2)

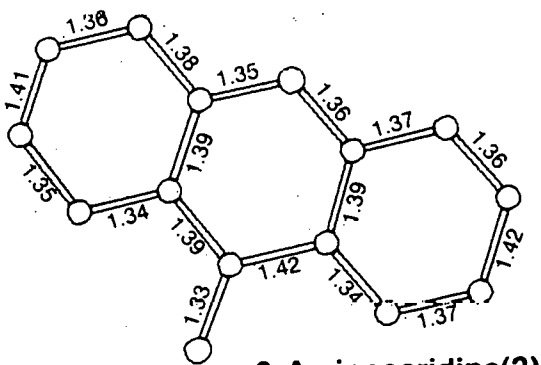

9-Aminoacridine(2)

Figure 5.

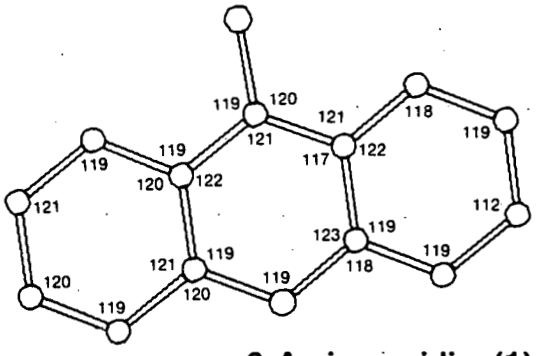

9-Aminoacridine(1)

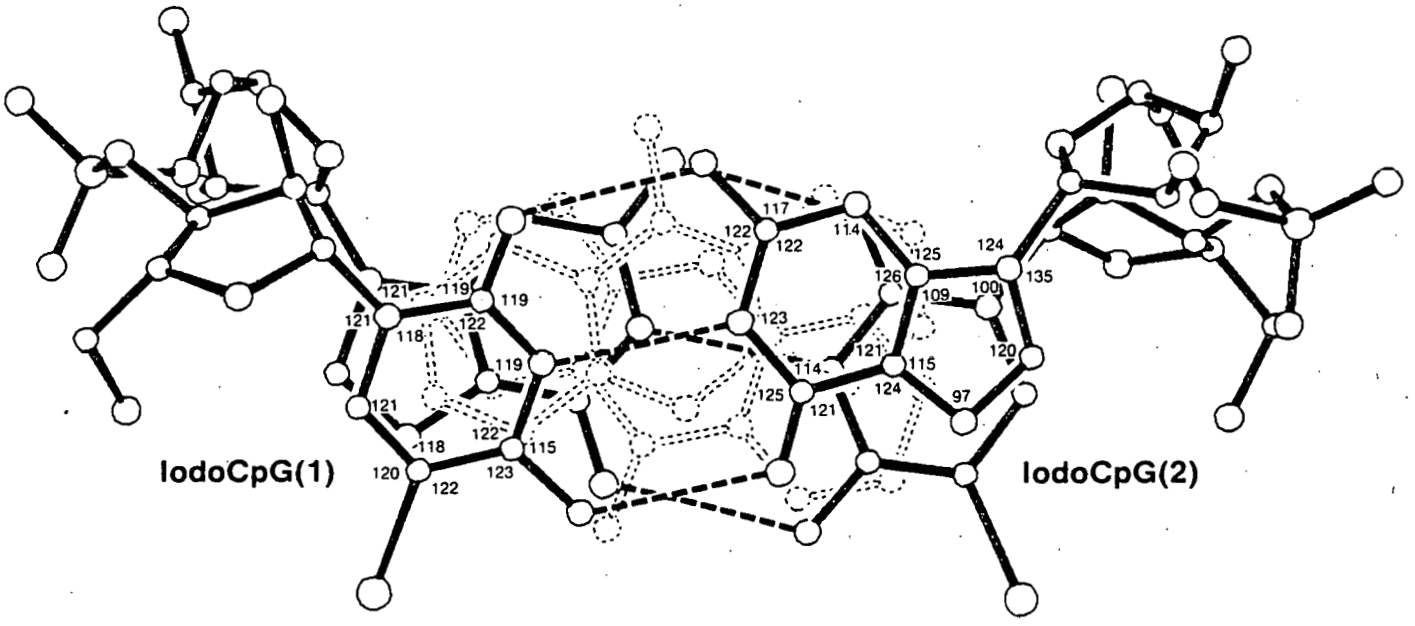

IodoCpG(1)

IodoCpG(2)

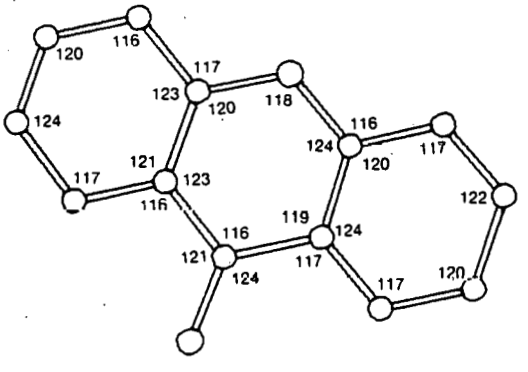

9-Aminoacridine(2)

Figure 6.

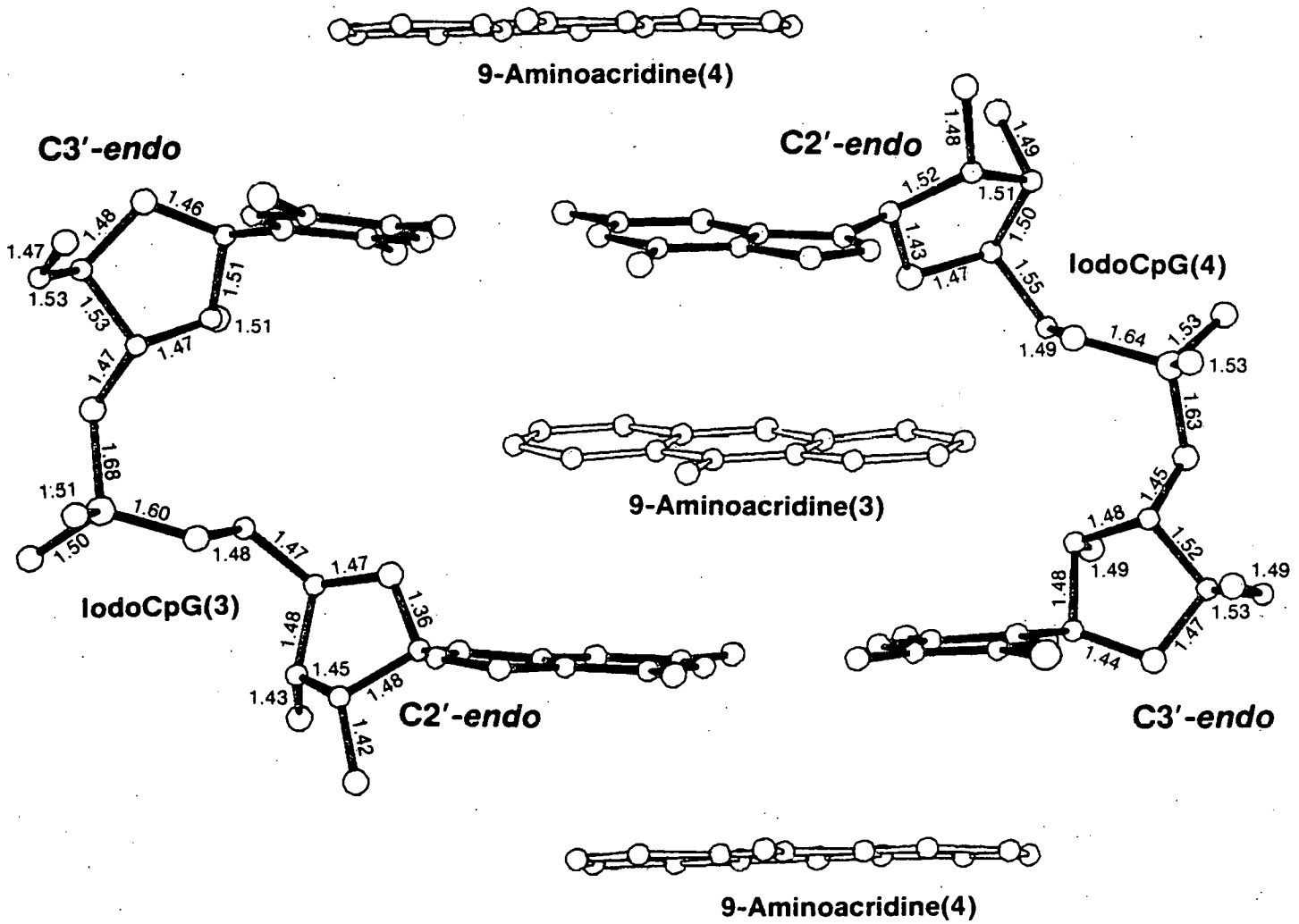
9-Aminoacridine(4)
C3′-endo
C2′-endo
IodoCpG(4)
9-Aminoacridine(3)
IodoCpG(3)
C2′-endo
C3′-endo
9-Aminoacridine(4)

Figure 7.

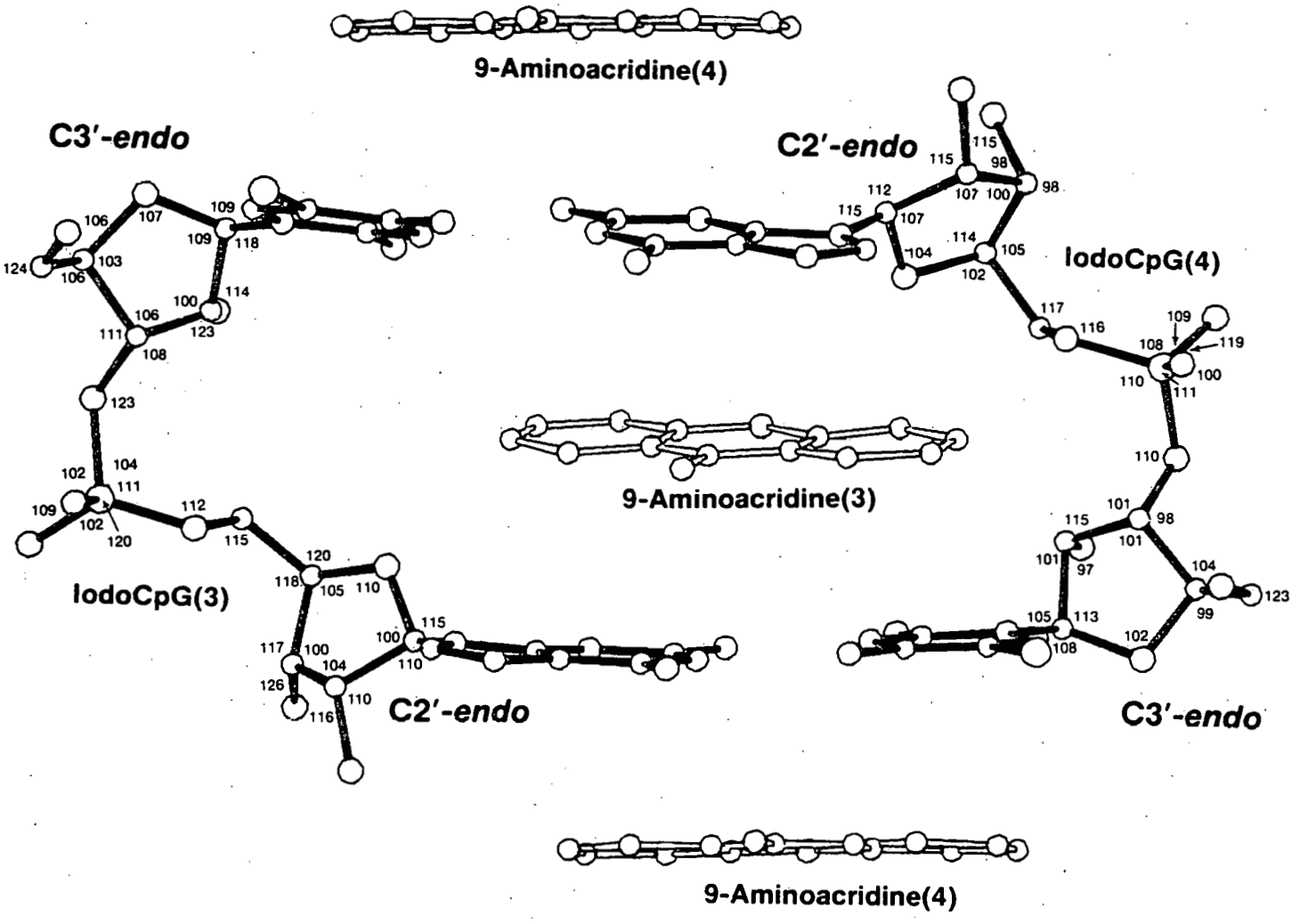
9-Aminoacridine(4)
C3′-endo
C2′-endo
IodoCpG(4)
9-Aminoacridine(3)
IodoCpG(3)
C2′-endo
C3′-endo
9-Aminoacridine(4)

Figure 8.

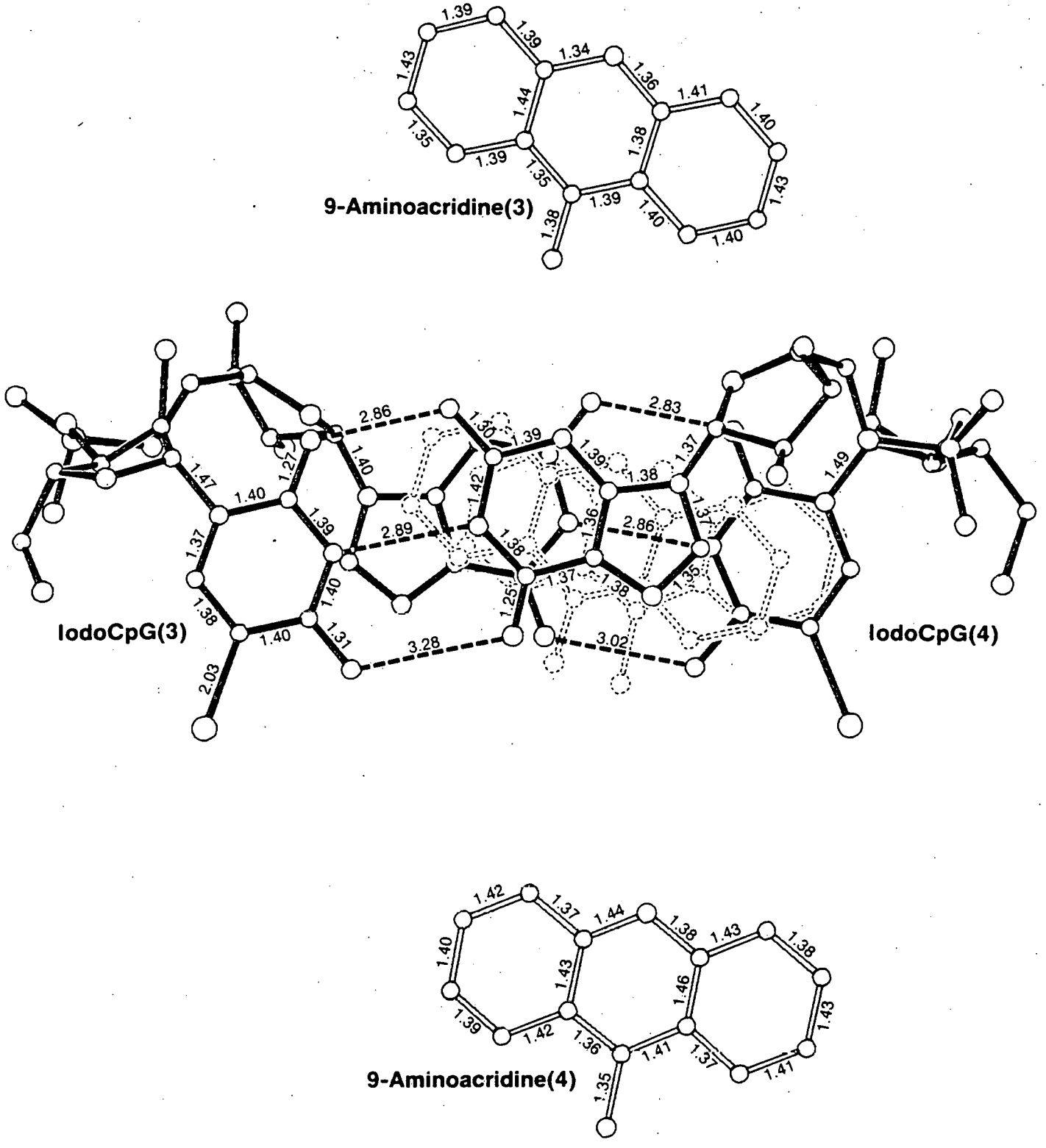

Figure 9.

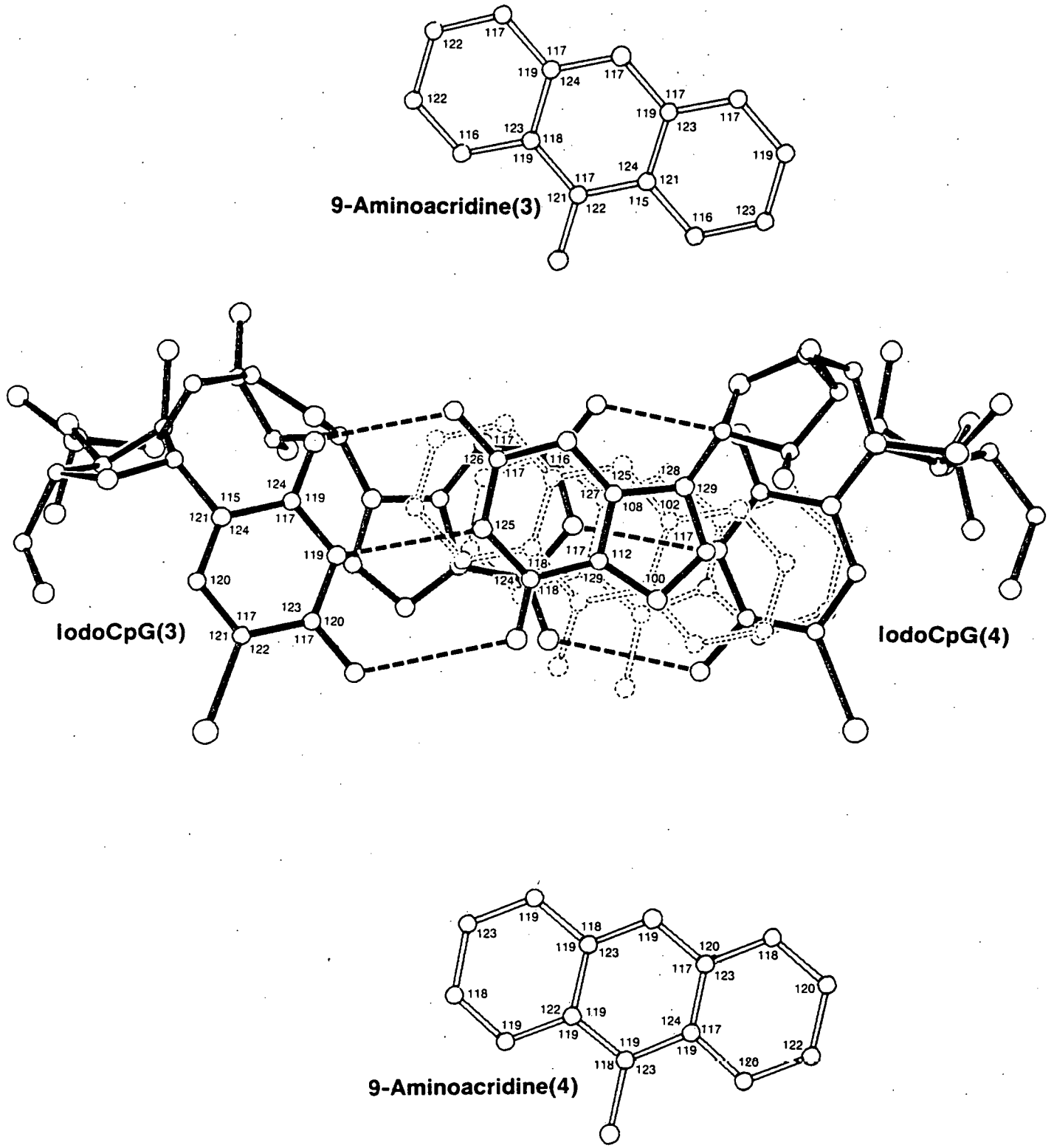

Figure 10.

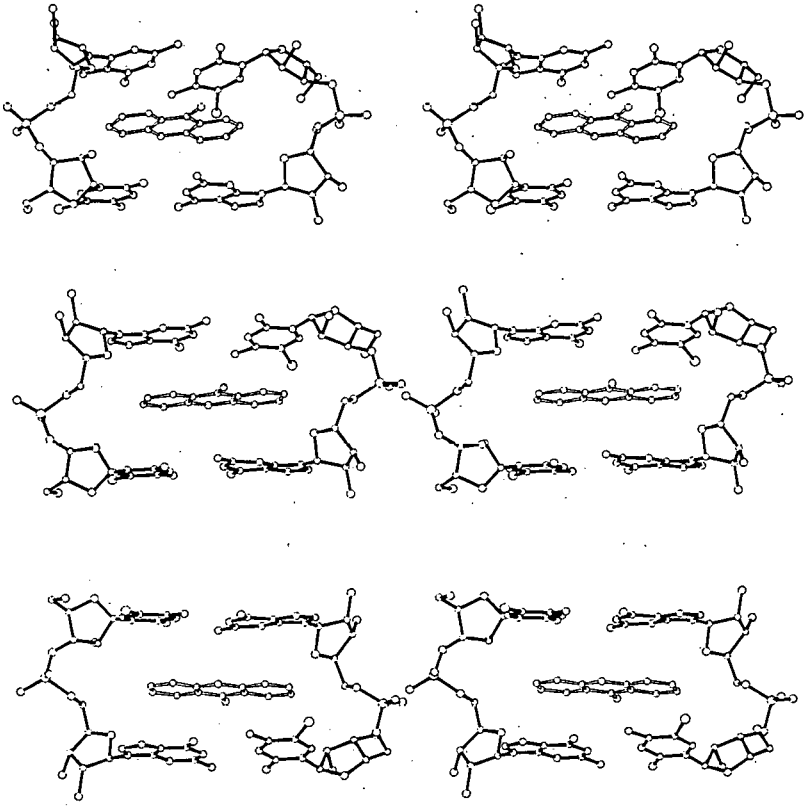

Figure 11.

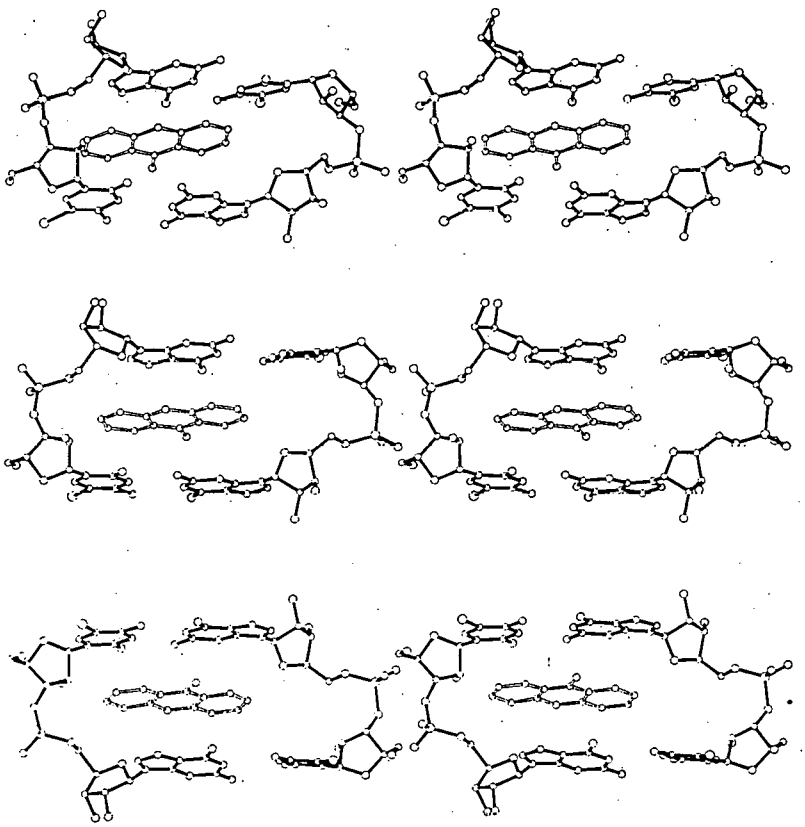

Figure 12.

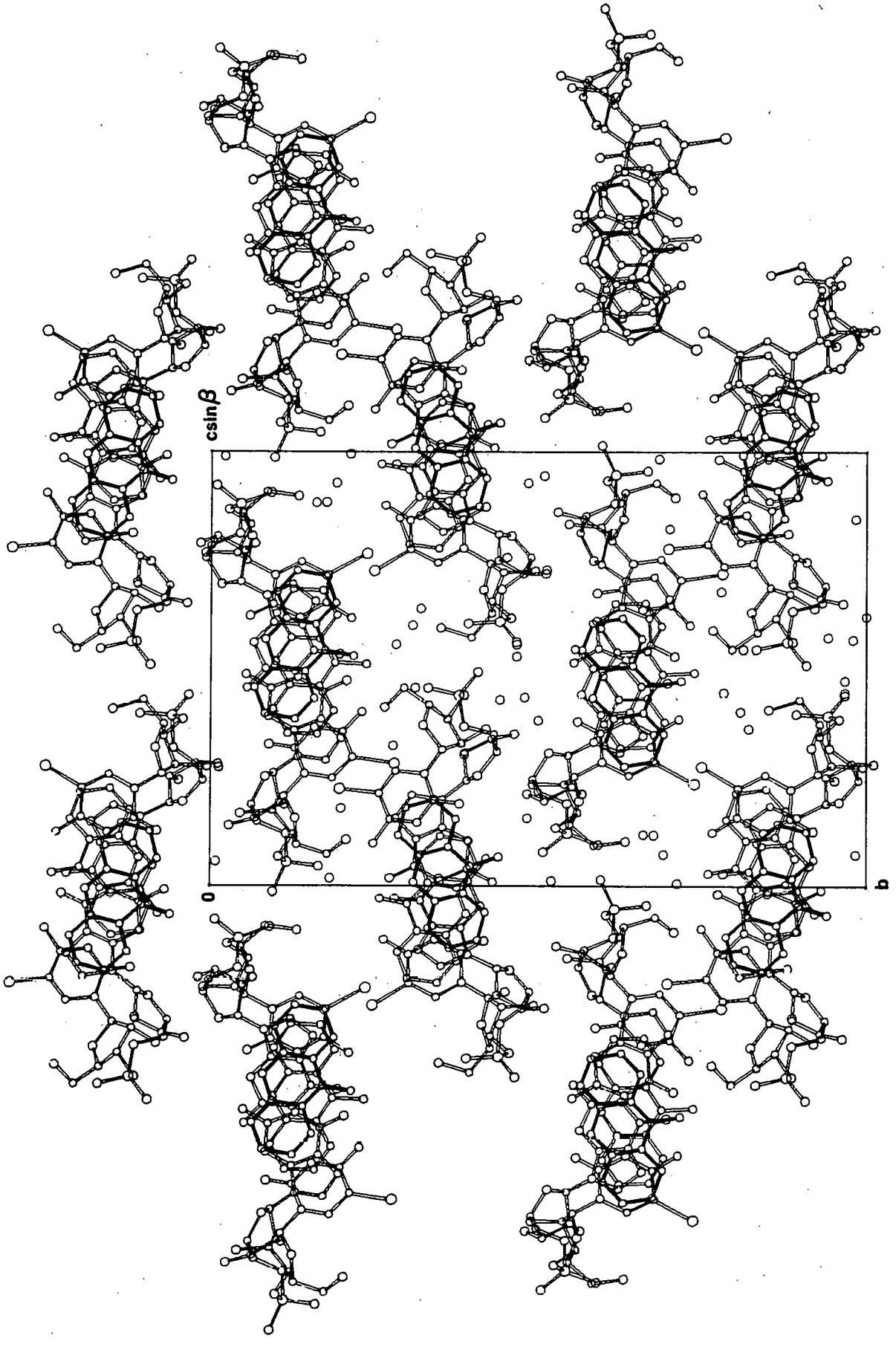

Figure 13.

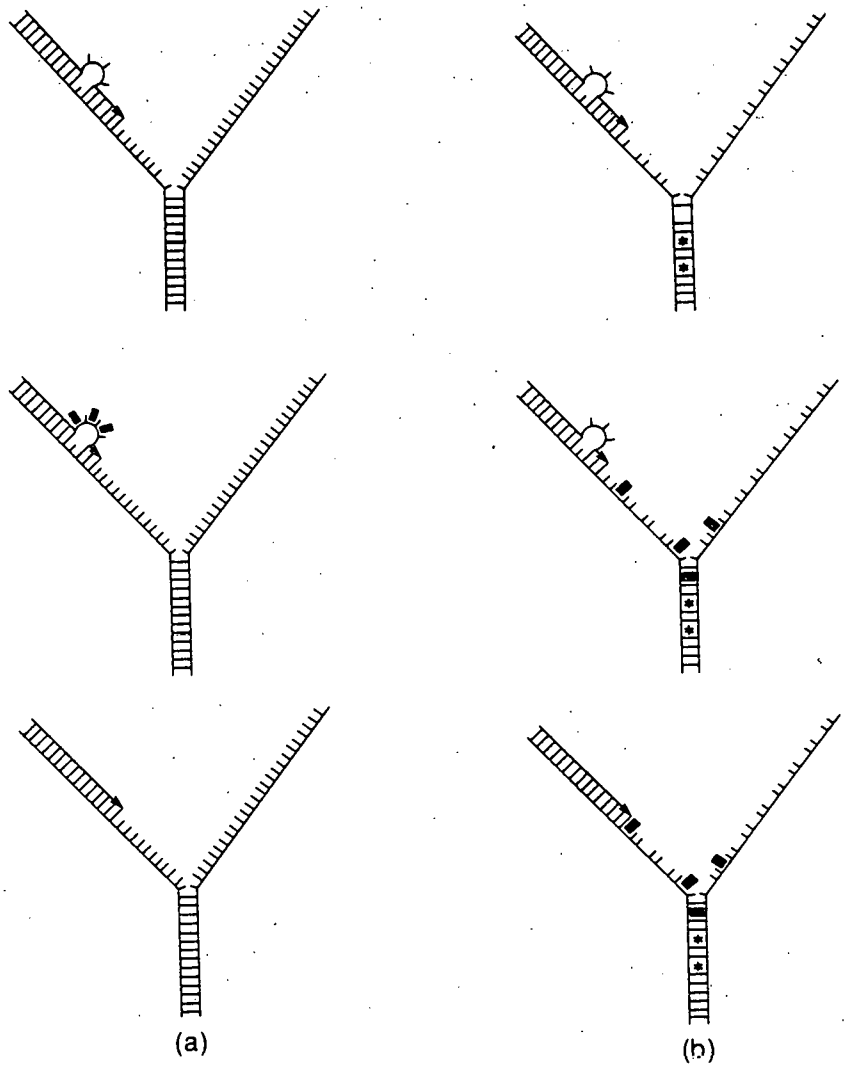

Figure 14.

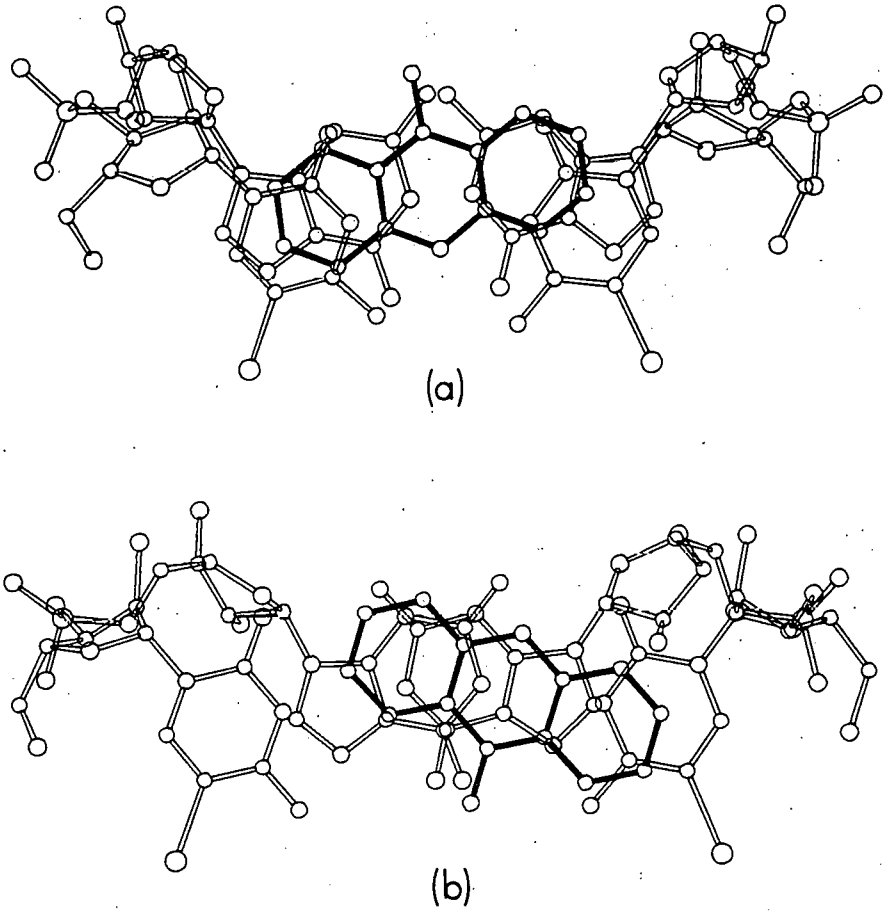

Figure 15.